A High Stopband-Rejection LTCC Filter With Multiple Transmission Zeros

Yng-Huey Jeng, *Student Member, IEEE*, Sheng-Fuh R. Chang, *Member, IEEE*, and Hsiao-Kuang Lin

***Abstract*—A low-temperature-cofired ceramic (LTCC) bandpass filter with high stopband rejection is presented for multistandard coexisted wireless communication applications, such as the integrated wireless local area network (WLAN)/wavelength code-division multiple access handset, the dual-band triple-mode WLANs, and the global system for mobile communications/global positioning system receivers. By improving the filter cell structure, $2n$ transmission zeros can be generated to achieve wide-band suppression from cascading n filter cells. The presented method provides the design flexibility of locating these transmission zeros distributed in the lower and upper stopbands. An LTCC bandpass filter with four transmission zeros has been implemented for experimental demonstration. The measured insertion loss is less than 1.5 dB at 2500 MHz, and four transmission zeros are obtained at 1.64, 1.88, 4.36, and 5.32 GHz, respectively. These result in 48–59 dB for lower stopband suppression and 38–55 dB for higher stopband reduction. This paper demonstrates that the proposed filter is extremely suitable for the multiband RF transceivers where the cross-band interference must be adequately reduced.**

***Index Terms*—Bandpass filters, image parameter, low-temperature-cofired ceramic (LTCC), stopband rejection.**

I. Introduction

THE development of multistandard coexisted mobile and wireless communications has been driving the RF transceiver to work at multiple different frequency bands since the coexisted wireless systems have their globally or regionally assigned operation frequency bands. For example, the wavelength code-division multiple access (WCDMA)/wireless local area network (WLAN) coexisted mobile terminal operates at 1.9 GHz for the WCDMA mode and 2.4 GHz for the WLAN mode. Thus, the RF transceiver architecture revolve from the conventional narrow-band architecture into various multiband forms, such as combined two narrow-band RF transceivers in parallel [1], [2] or concurrent architecture [3], [4]. This, in turn, requires new design considerations for both passive and active RF circuits of their original performance. Particularly for the RF band-selection bandpass filter, it must bear new requirement of stringent stopband suppression to reduce cross-band interference. This requirement becomes more difficult to be achieved when the operating frequencies of coexisted systems are close. Therefore, the bandpass filter with multiple arbitrary transmission zeros is necessary for use in the growing multiband RF transceivers.

In [5], the authors proposed a modified Chebeyshev bandpass filter to allow multiple transmission zeros that were arbitrarily distributed in the stopbands. Tang [6] adopted this schematic to design a 2.4-GHz bandpass filter with two transmission zeros in the lower stopband and one transmission zero in the upper stopband. By realizing the ten-layer low-temperature-cofired ceramic (LTCC) technology, the filter shows a good measured insertion loss of 2.0 dB, but the lower stopband transmission zeros are degenerated into one. Yeung and Wu [7] reported an LTCC bandpass filter with two transmission zeros based on the conventional schematic of a pair of inductive coupled resonators. The measurement results showed that two transmission zeros are located at the prescribed frequencies. Another work by Wada and Awai [8] employed the tapped half-wavelength open resonator to realize the Chebeyshev prototype and to generate two transmission zeros on each of the lower and upper stopbands. If n tapped half-wavelength resonators are used, there are $2n$ transmission zeros.

In this paper, a different design approach from the above methods [5]–[8] is presented based on the image-filter synthesis technique [9]–[11]. The approach cascades multiple elementary filter cells to achieve the desired specifications, where each cell can have the low-pass, high-pass, or band-pass response and is impedance-matched with its adjacent cells. To have advantageous stopband transmission zeros, new filter cells with inherent stopband transmission zeros are proposed. This design approach has fewer components than the circuits in [5]–[7] based on the comparison of the same number of transmission zeros. In Section II, the new filter cells having two transmission zeros are described. The design procedure is given in Section III. For the compact wireless transceiver applications in WCDMA/WLANs, a demonstrated bandpass filter with four transmission zeros is implemented using a multilayer LTCC technology. The cross-layer coupling effect, which is ignored in the proposed method, is included by three-dimensional (3-D) electromagnetic (EM) simulation. The measurement results are discussed in Section IV, and this paper is summarized in Section V.

II. Filter Cells With Two Transmission Zeros

By the image-filter synthesis technique, a bandpass filter can be easily synthesized with a cascade of double-m-derived filter cells [9]–[11]. The advantage is that this filter cell, which is illustrated in Fig. 1(a), provides two stopband transmission

Manuscript received April 18, 2005; revised September 27, 2005.

Y.-H. Jeng and S.-F. R. Chang are with the Department of Electrical Engineering and the Department of Communications Engineering, Center for Telecommunication Research, National Chung-Cheng University, Chia-Yi County 621, Taiwan, R.O.C. (e-mail: d8842004@ccu.edu.tw; ieesfc@ccu.edu.tw).

H.-K. Lin is with the RF Design Department, Fi-Win Corporation, Jhongli City 320, Taiwan, R.O.C. (e-mail: Shawn_Lin@fiwin.com.tw).

Digital Object Identifier 10.1109/TMTT.2005.862669

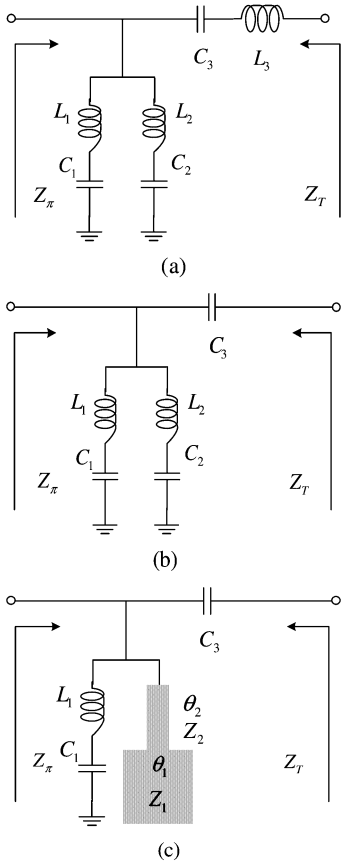

Fig. 1. Bandpass filter cells with two transmission zeros. (a) Conventional double-m cell. (b) Proposed cell with lumped elements. (c) Proposed cell with hybrid of lumped and distributed elements.

zeros. However, this topology has the drawback of unrealistic inductance value L_3 when implemented with the LTCC foundry process. Therefore, an enhanced filter cell without L_3, as shown in Fig. 1(b), is proposed. Furthermore, another form of the proposed filter cell is also investigated, which is a hybrid of distributed and lumped elements, as shown in Fig. 1(c).

A. Lumped Filter Cell

The $ABCD$ matrix of the lumped filter cell in Fig. 1(b) can be expressed as

$$\begin{bmatrix} A & B \\ C & D \end{bmatrix} = \begin{bmatrix} 1 & \frac{1}{j\omega C_3} \\ -j\omega C_3 \frac{Q_A}{Q_c} & \frac{Q_B}{Q_C} \end{bmatrix}$$

$$Q_B = \left(\frac{\omega^2}{\omega_{z1}^2} - 1\right)\left(1 - \frac{\omega^2}{\omega_{z2}^2}\right) + \frac{C_2}{C_3}\left(\frac{\omega^2}{\omega_{z1}^2} - 1\right) - \frac{C_1}{C_3}\left(1 - \frac{\omega^2}{\omega_{z2}^2}\right)$$

$$Q_A = \frac{C_1}{C_3}\left(1 - \frac{\omega^2}{\omega_{z2}^2}\right) - \frac{C_2}{C_3}\left(\frac{\omega^2}{\omega_{z1}^2} - 1\right)$$

$$Q_C = \left(\frac{\omega^2}{\omega_{z1}^2} - 1\right)\left(1 - \frac{\omega^2}{\omega_{z2}^2}\right) \tag{1}$$

where $\omega_{z1} = (1/\sqrt{L_1C_1})$ and $\omega_{z2} = (1/\sqrt{L_2C_2})$ denote the angular transmission-zero frequencies, which are generated from the series resonance of the shunt branches $L_1 - C_1$ and $L_2 - C_2$. At the transmission-zero frequencies, the input signal is totally reflected, resulting in infinite rejection. The circuit characteristics including the input image impedance Z_π, the output image impedance Z_T, and the transfer constant γ under the impedance match condition can be derived from (1) as follows:

$$Z_\pi = \sqrt{\frac{AB}{CD}} = \frac{Q_C}{\omega C_3\sqrt{Q_AQ_B}} \tag{2}$$

$$Z_T = \sqrt{\frac{BD}{AC}} = \frac{1}{\omega C_3}\sqrt{\frac{Q_B}{Q_A}} \tag{3}$$

$$\gamma \equiv \ln\frac{V_2}{V_1} = \sinh^{-1}\sqrt{BC} = \sinh^{-1}\sqrt{\frac{-Q_A}{Q_C}}. \tag{4}$$

For real power transfer to the matched load in the passband, the image impedances must be positive real and the transfer constant γ is purely imaginary. While in the stopband, the impedances are imaginary and the transfer constant γ becomes negative real. Therefore, from (2)–(4), the term D in (1) vanishes at a certain frequency named the transition frequency ω_c. By taking one step further, at the center angular frequency ω_0 of the passband, it is desired that the input impedance Z_π matches the source impedance R_S and the output impedance Z_T equals the load impedance R_L. Consequently, based on these criteria ($D(\omega_c) = 0, Z_\pi(\omega_0) = R_S$ and $Z_T(\omega_0) = R_L$) and the definitions of transmission zero, the circuit elements can be written in terms of $\omega_{z1}, \omega_{z2}, \omega_0, \omega_c, R_S$, and R_L as follows:

$$C_3 = \frac{1}{\omega_o R_L\sqrt{\frac{R_s}{R_L} - 1}} \tag{5}$$

$$C_1 = \frac{\left(1-\frac{\omega_{z1}^2}{\omega_o^2}\right)\left(\frac{\omega_c^2}{\omega_{z1}^2}-1\right)\left[\left(1-\frac{\omega_c^2}{\omega_{z2}^2}\right)-\left(1-\frac{R_L}{R_S}\right)\left(1-\frac{\omega_c^2}{\omega_{z2}^2}\right)\right]}{\omega_o R_L\sqrt{\frac{R_S}{R_L}-1}\left(1-\frac{\omega_c^2}{\omega_o^2}\right)\left(1-\frac{\omega_{z1}^2}{\omega_{z2}^2}\right)} \tag{6}$$

$$C_2 = \frac{\left(\frac{\omega_{z2}^2}{\omega_o^2}-1\right)\left(1-\frac{\omega_c^2}{\omega_{z2}^2}\right)\left[\left(\frac{\omega_c^2}{\omega_{z1}^2}-1\right)-\left(1-\frac{R_L}{R_S}\right)\left(\frac{\omega_o^2}{\omega_{z1}^2}-1\right)\right]}{\omega_o R_L\sqrt{\frac{R_S}{R_L}-1}\left(1-\frac{\omega_c^2}{\omega_0^2}\right)\left(\frac{\omega_{z2}^2}{\omega_{z1}^2}-1\right)} \tag{7}$$

$$L_1 = \frac{1}{\omega_{z1}^2 C_1} \tag{8}$$

$$L_2 = \frac{1}{\omega_{z2}^2 C_2}. \tag{9}$$

This set of equations will be used as the first-step circuit design under the prescribed filter specifications.

B. Hybrid Filter Cell

The shunt branch $L_1 - C_1$ (as well as $L_2 - C_2$) can be replaced by a step-impedance resonator, as shown in Fig. 1(c). The step-impedance resonator has the electric lengths θ_1 and θ_1 at ω_{z2} and the characteristic impedances Z_1 and Z_2 (let $k = Z_1/Z_2$). With the similar derivation as given in Section II-A, the $ABCD$ matrix and circuit elements can be obtained as follows:

$$\begin{bmatrix} A & B \\ C & D \end{bmatrix} = \begin{bmatrix} 1 & \frac{1}{j\omega C_3} \\ j\omega C_3\frac{-P_A}{\left(\frac{\omega^2}{\omega_{z1}^2}-1\right)} & \frac{P_B}{\left(\frac{\omega^2}{\omega_{z1}^2}-1\right)} \end{bmatrix} \tag{10}$$

$$P_A = \frac{jY_{\text{in}}}{\omega C_3}\left(\frac{\omega^2}{\omega_{z1}^2}-1\right)+\frac{C_1}{C_3}$$

$$P_B = -\left[\left(\frac{jY_{\text{in}}}{\omega C_3}-1\right)\left(\frac{\omega^2}{\omega_{z1}^2}-1\right)+\frac{C_1}{C_3}\right]$$

$$C_1 = \frac{\frac{\omega_c}{\omega_o}-\frac{\Theta_c}{\Theta_o}\left(1-\frac{R_L}{R_S}\right)}{\Omega_0 R_L\left(\frac{\Omega_c}{\Omega_0}-\frac{\Theta_c}{\Theta_o}\right)\sqrt{\frac{R_S}{R_L}-1}} \tag{11}$$

$$L_1 = \frac{1}{\omega_{z1}^2 C_1} \tag{12}$$

$$C_3 = \frac{1}{\omega_o R_L\sqrt{\frac{R_S}{R_L}-1}} \tag{13}$$

$$Z_2 = \frac{R_L\sqrt{\frac{R_S}{R_L}-1}\left(\frac{\Omega_c}{\Omega_o}\Theta_o-\Theta_c\right)}{\frac{\omega_c}{\omega_o}-\frac{\Omega_c}{\Omega_o}\left(1-\frac{R_L}{R_S}\right)} \tag{14}$$

$$\theta_2 = \tan^{-1}\left[k\cot\theta_1\right] \tag{15}$$

where

$$Y_{\text{in}} = j\frac{\tan\left(\theta_1\frac{f}{f_{z2}}\right)+k\tan\left(\theta_2\frac{f}{f_{z2}}\right)}{Z_2\left[k-\tan\left(\theta_1\frac{f}{f_{z2}}\right)\tan\left(\theta_2\frac{f}{f_{z2}}\right)\right]}$$

$$\Omega_o = \frac{\omega_o}{\left(\frac{\omega_o}{\omega_{z1}}\right)^2-1}$$

$$\Omega_c = \frac{\omega_c}{\left(\frac{\omega_c}{\omega_{z1}}\right)^2-1}$$

$$\Theta_o = \frac{\tan\left(\theta_1\frac{f_o}{f_{z2}}\right)+k\tan\left(\theta_2\frac{f_o}{f_{z2}}\right)}{k-\tan\left(\theta_1\frac{f_o}{f_{z2}}\right)\tan\left(\theta_2\frac{f_o}{f_{z2}}\right)}$$

$$\Theta_c = \frac{\tan\left(\theta_1\frac{f_c}{f_{z2}}\right)+k\tan\left(\theta_2\frac{f_c}{f_{z2}}\right)}{k-\tan\left(\theta_1\frac{f_c}{f_{z2}}\right)\tan\left(\theta_2\frac{f_c}{f_{z2}}\right)}.$$

C. Cascade of Filter Cells

Various types of bandpass filters with multiple transmission zeros can be constructed with cascade of above filet cells. If n filter cells are employed, $2n$ transmission zeros can be generated. The commonly used filter cells include π, T-type, double-π, and double-T architectures, where some of them are drawn in Fig. 2. The π- and T-type architectures have four transmission zeros while the double-π architecture has eight transmission zeros. Half of the transmission zeros are distributed over the lower stopband, and the other half are spread over the upper stopband.

III. Filter Design With LTCC Technology

To explain the circuit design details, an exemplary π-type and double-π bandpass filter is designed, and the π-type bandpass filter will be implemented with a seven-layer LTCC foundry. The design goal is a 2.4-GHz industrial–scientific–medical (ISM)-band WLAN/WPAN bandpass filter with high cross-band rejection of 45 dB at 1.8–1.9 GHz (GSM mobile) and 30 dB at 4.4–5.4 GHz (UWB). The design procedure is described in Section III-A.

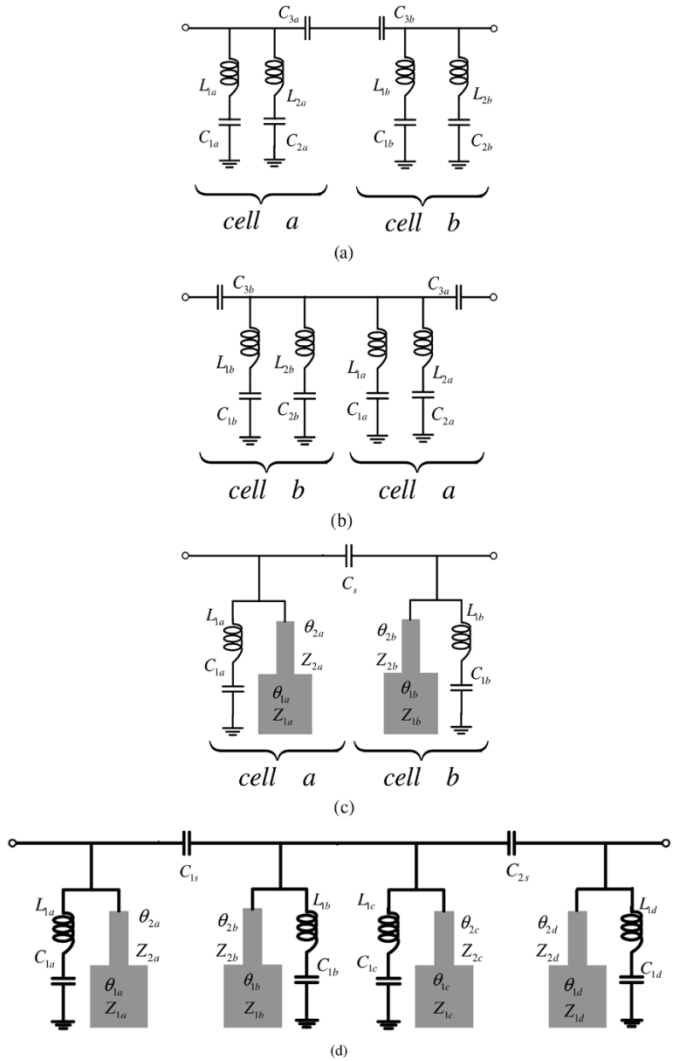

Fig. 2. Schematic diagram of bandpass filters. (a) Lumped-π. (b) Lumped T-type. (c) Hybrid-π. (d) Hybrid double-π.

A. Circuit Element Estimation and Calculated Spectral Response

The initial element values are calculated by selecting the following parameters:

- center frequency f_o: 2.45 GHz;
- low-band transmission zero frequencies f_{z1} and f_{z2}: 1.7 and 1.9 GHz;
- high-band transmission zero frequencies f_{z3} and f_{z4}: 4.25 and 5.25 GHz;
- cutoff frequency f_c: 2.3 GHz;
- input and output impedance: 50 Ω.

The 1.9- and 4.25-GHz transmission zeros are provided from Cell a and the 1.7- and 5.25-GHz transmission zeros are from Cell b. Substituting these parameters into (5)–(9), the element values are obtained and tabulated in Table I for the lumped-π structure. For the hybrid-π structure, we select $\theta_1 = 50^\circ$ and $k = 0.7$ for Cell a and $\theta_1 = 60^\circ$ and $k = 0.5$ for Cell b. Then,

TABLE I
ELEMENT VALUES OF THE LUMPED-π TYPE LTCC BANDPASS FILTER

C_{1a}	2.37 pF	L_{1a}	2.96 nH	f_{z1a}	1.90 GHz
C_{2a}	1.71 pF	L_{2a}	0.82 nH	f_{z2a}	4.25 GHz
C_{1b}	5.54 pF	L_{1b}	1.58 nH	f_{z1b}	1.70 GHz
C_{2b}	3.23 pF	L_{2b}	0.28 nH	f_{z2b}	5.25 GHz
C_{3a}	2.68pF	C_{3b}	2.68pF		

TABLE II
ELEMENT VALUES OF THE HYBRID-π TYPE LTCC BANDPASS FILTER

Z_{1a}	24.93 Ω	Z_{2a}	35.61 Ω	k	0.7
θ_{1a}	50^0	θ_{2a}	30.43^0	f_{z2a}	4.25 GHz
C_{1a}	2.48 pF	L_{1a}	2.83 nH	f_{z1a}	1.90 GHz
Z_{1b}	12.15 Ω	Z_{2b}	24.31 Ω	k	0.5
θ_{1b}	60^0	θ_{2b}	16.10^0	f_{z2b}	5.25 GHz
C_{1b}	5.14 pF	L_{1b}	1.704 nH	f_{z1b}	1.70 GHz
C_s	1.33 pF				

the other parameters, $\theta_2, Z_1, Z_2, C_1, L_1$, and C_3 are calculated by using (11)–(15). The element values are listed in Table II.

By substituting the estimated element values into the lumped-π, hybrid-π, and hybrid double-π networks in Fig. 2, their spectral responses can be obtained. The spectral characteristics of π circuits are drawn in Fig. 3(a). The calculated return loss is 32 dB. Four transmission zeros are generated at 1.7, 1.9, 4.25, and 5.25 GHz, thus satisfying the required stopband rejection. Both realizations by lumped elements and hybrid lumped and step-impedance resonators have almost identical spectral responses. This shows that both lumped-π and hybrid-π networks can achieve the prescribed filter response and provide the designer with an option to choose available components in implementation. In Fig. 3(b), where double-π circuitry is used, eight transmission zeros are distributed over both the lower and upper stopbands such that a high stopband rejection can be achieved over a wide frequency range.

B. LTCC Layout

For experimental verification, the hybrid-π circuit is implemented on a seven-layer LTCC substrate, which has a dielectric constant ε_r of 7.8, loss tangent of 0.0043, and a dielectric layer thickness of 90–90–135–90–90–90–180 μm consecutively from the top. The layout and the microphotograph are shown in Fig. 4, where the circuit size is 5.4 mm × 3.9 mm × 0.765 mm. The coupling capacitor C_s is implemented in layers 1 and 2 using the metal–insulator–metal (MIM) structure. Two inductors L_1 and L_2 using the planar spiral structure are located on layer 3. The capacitors C_{1a} and C_{1b} are formed by layer 5 with the ground layers 4 and 6, where C_{1a} is implemented with the MIM structure and C_{1b} with the vertically interdigital-capacitor (VIC) structure. The step-impedance resonators are placed on layer 7, which are shielded with two neighboring layers (6 and 7b) to minimize the interaction with other components.

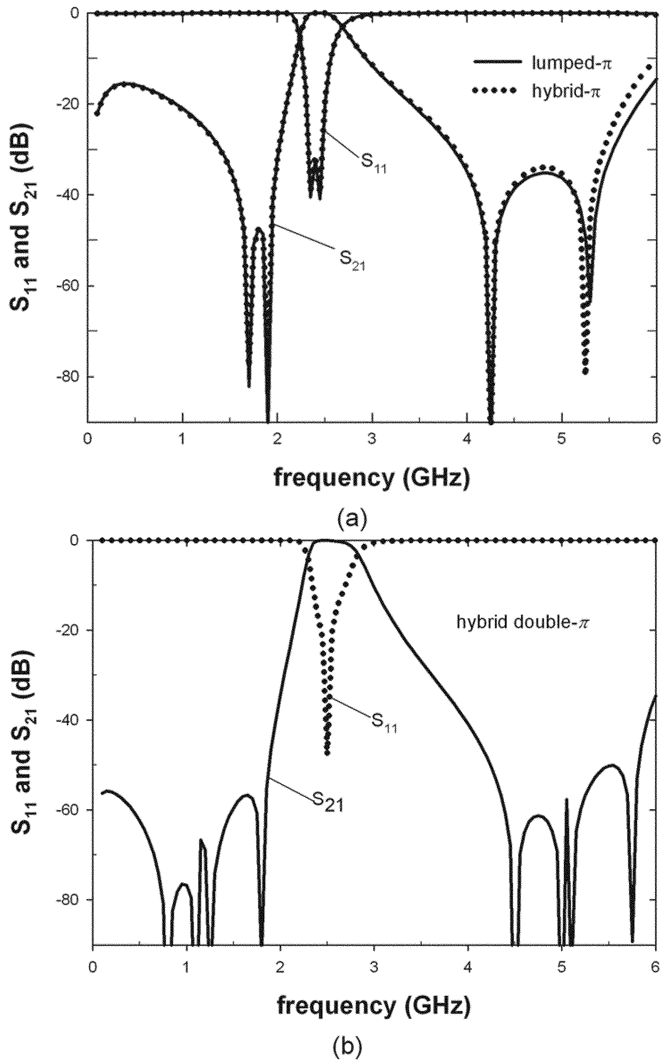

Fig. 3. Calculated spectral response with the proposed method. (a) Lumped-π and hybrid-π network. (b) Hybrid double-π network.

C. 3-D EM Simulation for Including Substrate Losses and Cross-Layer Coupling

To include the dielectric and conductor losses and the cross-layer spurious coupling in the LTCC multilayer structure, a 3-D EM simulator HFSS[1] was conducted. It was found from the simulation that the parasitic ground capacitance C_s is on the order of subpicofarads, which will considerably affect the correct C_s value and the step-impedance-resonator dimensions, as estimated in Section III-A. Therefore, each component dimension is fine-tuned to have the correct passband and satisfied insertion loss and stopband rejection.

Fig. 5 compares the calculation results, based on the proposed method, with the HFSS simulation results. The calculation results of the hybrid-π LTCC bandpass filter are illustrated by the dotted line, and the HFSS simulation results are drawn by the solid line in Fig. 5. The HFSS simulation results demonstrate a 1.8-dB insertion loss and a 15-dB return loss at 2450 MHz. The four transmission zeros are observed at 1.6, 1.9,

[1] HFSS v9.1, Ansoft Corporation, Pittsburgh, PA, 2003.

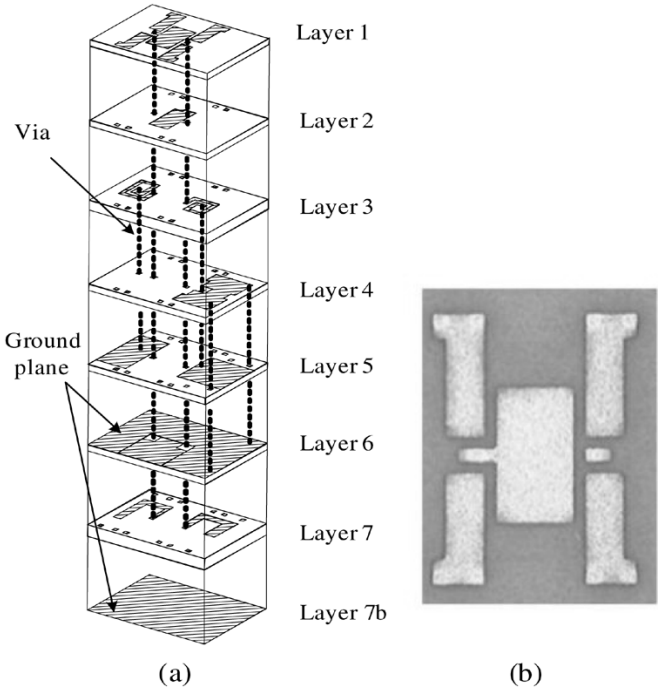

Fig. 4. Designed 2.45-GHz hybrid-π bandpass filter. (a) LTCC layout. (b) Microphotograph.

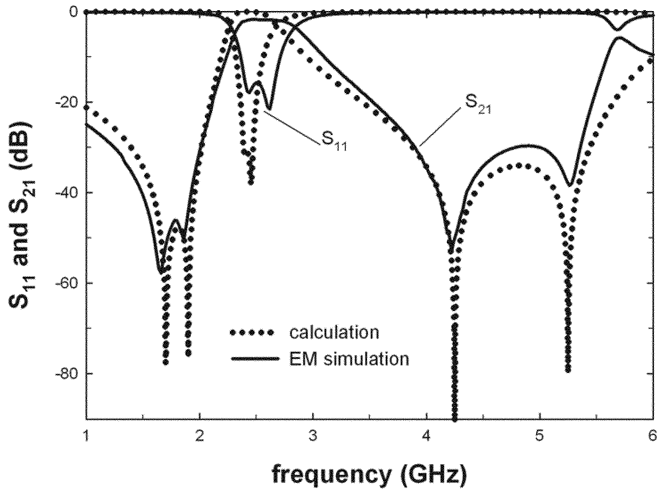

Fig. 5. Comparison of the calculation results (based on our proposed method) and the HFSS simulation results.

4.2, and 5.25 GHz, respectively. The calculation and EM simulation agree very well in overall frequency response. Nevertheless, the passband bandwidth slightly widens in simulation due to the conductor and dielectric losses and the cross-layer coupling in the LTCC structure, which can be taken into account by HFSS simulation but ignored in the derived equations (5)–(9) and (11)–(15).

IV. Measurement Results and Discussion

The ground–signal–ground (G–S–G) probes with 250-μm pitch are used for on-chip measurement, which are connected to the vector network analyzer for obtaining scattering parameters.

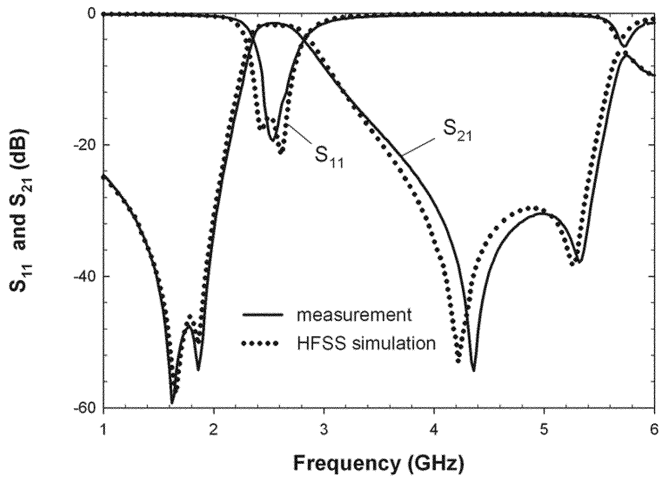

Fig. 6. Simulation and measurement results of the 2.45-GHz hybrid-π bandpass filter.

The measured insertion loss is less than 1.5 dB, and the return loss is better than 15 dB at 2500 MHz for Fig. 6. The four transmission zeros are measured at 1.64, 1.88, 4.36, and 5.32 GHz, respectively. Although the two higher transmission-zeros frequencies are slightly up-shifted, their resultant stopband rejection is not deteriorated. In the low band of 1.6–1.9 GHz, the stopband suppression of 48–59 dB is achieved and, in the high band of 4.1–5.4 GHz, suppression of 31–55 dB is obtained. The measurement results agree very well with the 3-D simulation, showing that the proposed design method is very effective in high-performance LTCC bandpass filter design.

V. Conclusion

An LTCC bandpass filter with high stopband rejection is presented based on the image-filter synthesis method for multiband RF transceivers in the multistandard coexisted wireless communication. New filter cell structures with stopband transmission zeros, which are suitable for the LTCC foundry process, are analyzed such that a compact LTCC bandpass filter with $2n$ stopband transmission zeros can be accurately designed by the cascaded combination of n such cells. These $2n$ transmission zeros can be arbitrarily distributed in the lower and upper stopbands. The advantage of the proposed method provides a set of accurate and explicit equations for element value estimation to achieve the required filter specifications. Then, these values are substituted into an EM simulator for fine-tuning to include the LTCC substrate conductor losses and cross-layer coupling. An LTCC hybrid-π bandpass filter has been implemented for WCDMA/WLAN coexisted application. In the range of 2400–2500 MHz, the measured insertion loss is less than 1.5 dB and the return losses are better than 15 dB. Four transmission zeros are obtained at 1.64, 1.88, 4.36, and 5.32 GHz, respectively, which results in 48–59 dB lower stopband suppression and 31–55 dB upper stopband suppression. These promising results demonstrate that the proposed filter has great application potential in multiband RF transceivers, where the stringent cross-band interference suppression is required.

REFERENCES

[1] S. Wu and B. Razavi, "A 900-MHz/1.8-GHz CMOS receiver for dual-band applications," *IEEE J. Solid-State Circuits*, vol. 33, no. 12, pp. 2178–2185, Dec. 1998.

[2] J. Tham, M. Margrait, B. Pregardier, C. Hull, R. Magoon, and F. Carr, "A 2.7 V 900-MHz dual-band transceiver IC for digital wireless communications," *IEEE J. Solid-State Circuits*, vol. 34, no. 3, pp. 282–291, Mar. 1999.

[3] H. Hashemi and A. Hajimiri, "Concurrent multiband low-noise amplifiers-theory, design, and applications," *IEEE Trans. Microw. Theory Tech.*, vol. 50, no. 1, pp. 288–301, Jan. 2002.

[4] S. F. Chang, W. L. Chen, S. C. Chang, C. K. Tu, C. L. Wei, C. H. Chien, C. H. Tsai, J. Chen, and A. Chen, "A dual-band RF transceiver for multistandard WLAN applications," *IEEE Trans. Microw. Theory Tech.*, vol. 50, no. 2, pp. 1048–1055, Feb. 2005.

[5] J. S. Lim and D. C. Park, "A modified Chebyshev bandpass filter with attenuation poles in the stopband," *IEEE Trans. Microw. Theory Tech.*, vol. 45, no. 6, pp. 898–904, Jun. 1997.

[6] C.-W. Tang, "Harmonic-suppression LTCC filter with the step-impedance quarter-wavelength open stub," *IEEE Trans. Microw. Theory Tech.*, vol. 52, no. 2, pp. 617–624, Feb. 2004.

[7] L. K. Yeung and K. L. Wu, "A compact second-order LTCC bandpass filter with two finite transmission zeros," *IEEE Trans. Microw. Theory Tech.*, vol. 51, no. 2, pp. 337–341, Feb. 2003.

[8] K. Wada and I. Awai, "Design of a bandpass filter with multiple attenuation poles based on tapped resonators," *IEICE Trans. Electron*, vol. E82-C, no. 7, pp. 1116–1122, Jul. 1999.

[9] T. H. Shea, *Transmission Networks and Wave Filters*. New York: Van Nostrand, 1930.

[10] G. L. Matthaei, L. Young, and E. M. T. Jones, *Microwave Filters, Impedance-Matching Networks, and Coupling Structures*. Dedham, MA: Artech House, 1980.

[11] M. Hasler and J. Neirynck, *Electric Filters*. Boston, MA: Artech House, 1986.

Yng-Huey Jeng (S'05) received the M.S. degree in physics from National Chung-Cheng University, Douliou City, Taiwan, R.O.C., in 1997, and is currently working toward the Ph.D. degree at National Chung-Cheng University.

Her research interests include microwave filter in LTCC and organic substrates and high-power microwave sources.

Sheng-Fuh R. Chang (S'83–M'92) received the B.S. and M.S. degrees in communications engineering from National Chiao-Tung University, Hsinchu, Taiwan, R.O.C., in 1982 and 1984, respectively, and the Ph.D. degree in electrical engineering from the University of Wisconsin–Madison, in 1991.

He was involved with high-power microwave and millimeter-wave sources such as free-electron lasers and Cherenkov masers at the Center for Plasma Theory and Computation, University of Wisconsin–Madison. In 1992, he joined the Hyton Technology Corporation, where he was responsible for C- and Ku-band satellite low-noise down-converters and multichannel multipoint distribution system (MMDS) transceivers. In 1994, he joined the Department of Electrical Engineering, National Chung-Cheng University, Douliou City, Taiwan, R.O.C., where he is currently a Full Professor with the Department of Electrical Engineering and is also the Vice Director of the Center for Telecommunication Research. His research interests include microwave and millimeter-wave integrated circuits with CMOS, heterojunction bipolar transistor (HBT), and pseudomorphic high electron-mobility transistor (pHEMT) technologies, multifunctional RF transceivers, smart-antenna RF system, and high-power microwave sources.

Prof. Chang is a member of Phi Tau Phi and Sigma Xi.

Hsiao-Kuang Lin was born in Miaoli, Taiwan, R.O.C., in 1979. He received the M.S. degree in electrical engineering, National Chung-Cheng University, Douliou City, Taiwan, R.O.C., in 2004.

He is currently a Research and Development Engineer with the RF Design Department, Fi-Win Corporation, Jhongli City, Taiwan, R.O.C. His research interests are WLAN communication systems.